Advances in the Steady-State Hybrid Regime in DIII-D – a Fully-Noninductive, ELM-Suppressed Scenario for ITER

C.C. Petty[1], R. Nazikian[2], F. Turco[3], Xi Chen[1], T.E. Evans[1], N.M. Ferraro[2], J.R. Ferron[1], A.M. Garofalo[1], B.A. Grierson[2], C.T. Holcomb[4], A.W. Hyatt[1], E. Kolemen[2], R.J. La Haye[1], C. Lasnier[4], N. Logan[2], T.C. Luce[1], D. Orlov[5], T.H. Osborne[1], D.C. Pace[1], C. Paz-Soldan[1], T.W. Petrie[1], P.B. Snyder[1], W.M. Solomon[1], N.Z. Taylor[1], K.E. Thome[6], M.A. Van Zeeland[1] and Y. Zhu[7]

[1]General Atomics, PO Box 85608, San Diego, CA 92186-5608, USA
[2]Princeton Plasma Physics Laboratory, 100 Stellarator Rd., Princeton, NJ 08540, USA
[3]Columbia University, 2960 Broadway, New York, NY 10027-6900, USA
[4]Lawrence Livermore National Laboratory, 7000 East Ave, Livermore, CA 94550, USA
[5]University of California San Diego, 9500 Gilman Dr., La Jolla, CA 92093, USA
[6]Oak Ridge Associated Universities, PO Box 117, Oak Ridge, TN 37831, USA
[7]University of California Irvine, Irvine, CA 92697, USA

E-mail contact of main author: petty@fusion.gat.com

Abstract. A new ELM suppression regime has been attained in the fully-noninductive hybrid scenario in DIII-D with beta, collisionality and plasma shape relevant to the ITER steady-state mission. Fully noninductive hybrids with high beta ($\langle\beta\rangle \leq 2.8\%$) and high confinement ($H_{98y2} \leq 1.4$) in the ITER similar shape have achieved zero surface loop voltage for ≤ 2 current relaxation times using efficient central current drive from ECCD and NBCD. For the first time, this steady-state regime has been successfully integrated with ELM suppression by applying an odd parity n=3 magnetic perturbation; the strong resonant interaction allows ELM suppression over a wide range of q_{95} (6 – 7.5) with little pedestal degradation. High beta hybrid plasmas are also integrated with an Argon-based radiative divertor to advance divertor heat flux dissipation towards reactor relevance.

1. ITER-Relevant, Steady-State Hybrids

Experiments in DIII-D are developing a steady-state hybrid scenario with strong central current drive and q_{min} slightly above unity [1,2], where the "hybrid" regime refers to a stationary, high performance H-mode scenario that has higher confinement and greater stability to the m/n=2/1 tearing mode than the conventional H-mode regime. A joint report has been published from four large divertor tokamaks on the physics basis of the hybrid scenario and prospects for applications in ITER [3]. In DIII-D, the favorable properties of hybrids are largely attributed to the presence of a small m/n=3/2 tearing mode that prevents sawteeth by raising q_{min} slightly above 1 with low central magnetic shear [4]. This removes a trigger mechanism for the deleterious m/n=2/1 tearing mode, while the low magnetic shear is beneficial in reducing heat transport [5]. The anomalously broad current profile is an important feature of the steady-state hybrid regime, as the decoupling between the plasma current profile and the current drive profile allows the latter to be located near the plasma center where the current drive efficiency is highest.

An exciting new development in steady-state hybrid research is the integration of ELM suppression with a high-beta, fully-noninductive plasma in the ITER similar shape. Type-I ELMs cannot be tolerated in future fusion reactors owing to the large anticipated erosion and dangerous cyclic thermal stresses expected on plasma facing components [6]. Figure 1 shows the integration of a steady-state hybrid discharge with ELM suppression by applying an n=3 RMP from the I-coil with odd parity. The fully noninductive period of the discharge, with average values of $\beta_N = 3.0$, $\beta_P = 1.9$ and $H_{98y2} = 1.2$ using 3.5 MW of ECCD power and 9.9 MW of NBCD power, is limited only by the neutral beam duration. The noninductive current

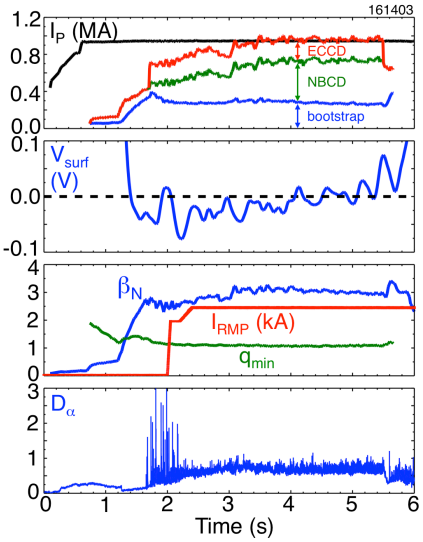

FIG. 1. Fully noninductive hybrid with RMP ELM suppression.

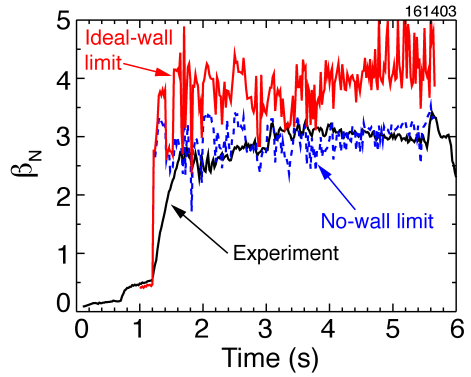

FIG. 2. Comparison of measured β_N with DCON stability calculations.

TABLE 1. CURRENT AND LOOP VOLTAGE FOR STEADY-STATE HYBRIDS WITH AND WITHOUT RMP ELM SUPPRESSION.

	With RMP (Shot 161403)	Without RMP (Shot 161418)
ECCD	0.23 MA	0.22 MA
NBCD	0.46 MA	0.46 MA
Bootstrap	0.27 MA	0.28 MA
Plasma current	0.95 MA	0.95 MA
Loop voltage	0±3 mV	-3±4 mV

drive, plasma stability, core transport, etc., are little affected by the RMP. Importantly, the plasma parameters for these discharges in DIII-D extrapolate well to the expected conditions for ITER's steady-state mission (see Sec. 5).

A significant feature of hybrids with a m/n=3/2 tearing mode is that the current profile is anomalously broad. A novel technique has been developed to quantify this anomaly by looking at the difference between the poloidal flux provided by the coils and the poloidal flux converted to kinetic energy in the plasma [7]. Without the 3/2 mode, these two poloidal flux measurements agree, but with the 3/2 mode the conversion of poloidal flux into kinetic energy is larger by 0.02 Wb/s, which is significant since the equivalent loop voltage would drive ~10% of the plasma current. This difference remains around 0.02 Wb/s regardless of whether or not RMP ELM suppression is used. This poloidal flux anomaly may be consistent with the formation of an electrostatic dynamo EMF arising from the helical core equilibria [8].

Fully noninductive conditions are readily achieved in hybrids both with and without RMP ELM suppression. Table I gives the calculated values of the noninductive currents and measured surface loop voltages for both a RMP ELM-suppressed hybrid and a matched non-RMP hybrid. Despite the centrally peaked current drive from ECCD and NBCD, q_{min} anomalously remains above 1 for the duration of the discharge (the current relaxation time is τ_R = 1.9 s and TRANSP modeling predicts that q_{min} should drop to 0.7).

Stability calculations show that the achieved β_N for these steady-state hybrids equals the no-wall n=1 stability limit while remaining well below the ideal with-wall n=1 limit, as shown in Fig. 2. The no-wall limit calculated by DCON ranges from $\approx 3.1\ell_i$ early in the high beta phase to $\approx 3.5\ell_i$ late in high beta phase. The ideal with-wall n=1 limit also increases slowly with time and has an average value of $\beta_N \approx 4.0$, indicating that higher beta operation should be possible in this RMP ELM-suppressed, steady-state hybrid regime with increased heating power.

2. ELM Suppression Physics in Fully-Noninductive Plasmas

Analysis suggests that weakly-damped, positive-reluctance modes in the plasma edge are responsible for the favorable characteristics of ELM suppression in these steady-state hybrid plasmas. Reluctance relates the external perturbed flux to the effective perturbed plasma

current. In ITER Baseline plasmas, Type-I ELM suppression is achieved for narrow windows in q_{95} via the excitation of strongly-damped edge kink modes with negative reluctance [9,10]. These modes can only drive modest currents at edge rational surfaces, so that a strong RMP (I_{coil} = 4.4 kA) is needed to generate the J×B torque required to drive islands at the top of the pedestal [11]. Surprisingly, ELM suppression is more easily obtained in steady-state hybrid plasmas with modest RMP amplitude (I_{coil} = 2.5 kA) over a wide range of q_{95} (6 – 7.5) and with minimal confinement degradation (≈5%). These plasmas have weakly-stable edge localized modes with positive reluctance (i.e., amplifying modes), analogous to the Resonant Field Amplification (RFA) of stable resistive wall modes at high beta. In principle, the control of such weakly stable modes at high beta enables the use of small nonaxisymmetric fields to achieve the resonant field amplitudes required for suppression. This will be particularly important in future reactors where maximizing the plasma response will minimize the required external magnetic perturbation to achieve ELM suppression.

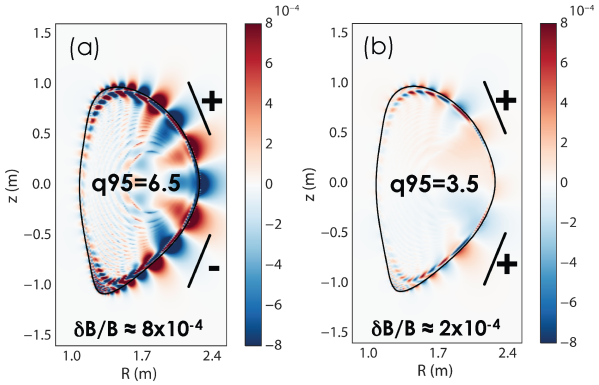

FIG. 3. IPEC calculations of n=3 RMP with 1 kA coil current for (a) odd parity and (b) even parity.

MHD calculations show that the excitation of (1) a weakly-stable edge kink mode at high beta and (2) a high density of edge rational surfaces combine to produce an island chain that maintains suppression over a wide range in q_{95}. The first point is demonstrated in Fig. 3, which compares the IPEC [12] calculated linear ideal MHD plasma response for I_{coil} = 1 kA for a steady-state hybrid plasma ($\beta_N \approx 3.0$, $q_{95} \approx 6.5$, n=3 odd parity) and an ITER Baseline plasma ($\beta_N \approx 1.8$, $q_{95} \approx 3.5$, n=3 even parity). The odd parity configuration couples well to the high-q_{95} steady-state case, whereas the even parity configuration couples better to the low-q_{95} baseline scenario. The hybrid case shows an edge localized plasma response that is strongly amplified and outward ballooning, indicative of a weakly-damped n=3 edge kink mode, whereas the edge plasma response is much weaker for the ITER Baseline case, indicative of the excitation of a highly-damped edge mode. The much stronger kink response in the hybrid plasma leads to stronger screening currents on edge rational surfaces. Figure 4 shows the resonant coupling to each rational surface for the hybrid and ITER Baseline cases from the IPEC analysis. The much stronger resonant coupling to the plasma edge in the hybrid is a consequence of the excitation of a weakly-damped edge mode compared to a strongly-damped mode in the ITER Baseline. A single positive-reluctance mode can account for most of the edge plasma response seen in the hybrid plasma. This positive-reluctance mode differs qualitatively from the more anemic edge response of the highly-stable, negative-reluctance modes for the ITER Baseline.

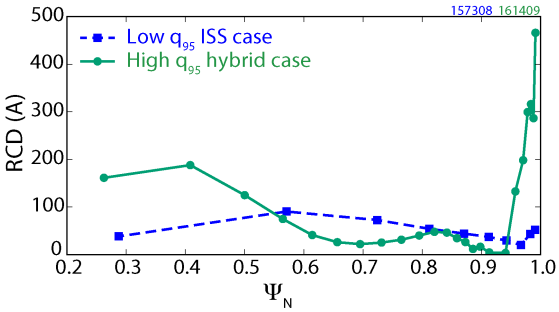

FIG. 4. Resonant field amplitude δBr on rational surfaces calculated for even parity (blue) and odd parity (green) n=3 RMP.

The combination of a strongly-driven edge-kink response with a high density of edge rationals at high q_{95} should lead to the formation of a magnetic island chain that can account for the wide q_{95} window for ELM suppression observed in steady-state hybrid plasmas. Figure 5 plots the linearly calculated Chirikov parameter for island overlap with I_{coil} = 1 kA using the extended-MHD code M3D-C1 [13] for the hybrid plasma. The Chirikov parameter equals or

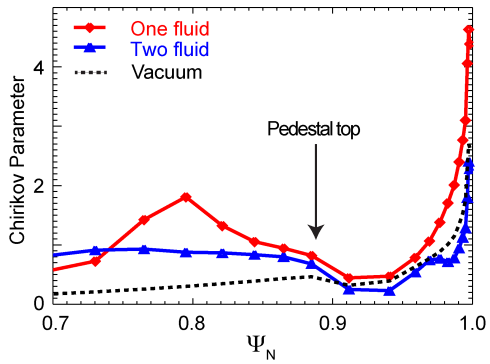

FIG. 5. Linear M3D-C1 calculation of Chirakov parameter for steady-state hybrid plasma.

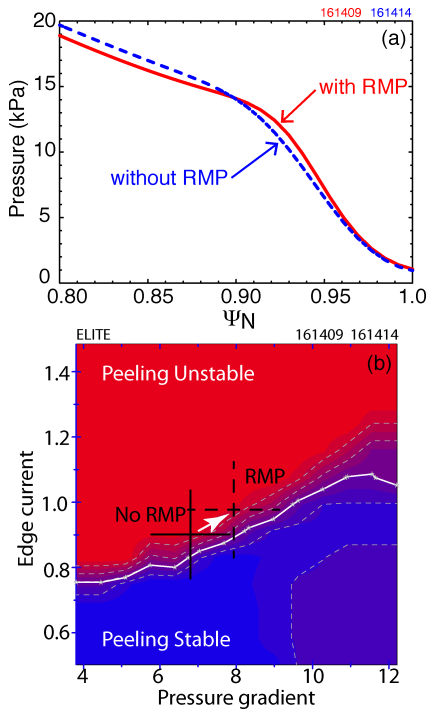

FIG. 6. (a) Measured pedestal pressure profile with and without odd parity n=3 RMP. (b) Peeling-ballooning stability calculated using ELITE.

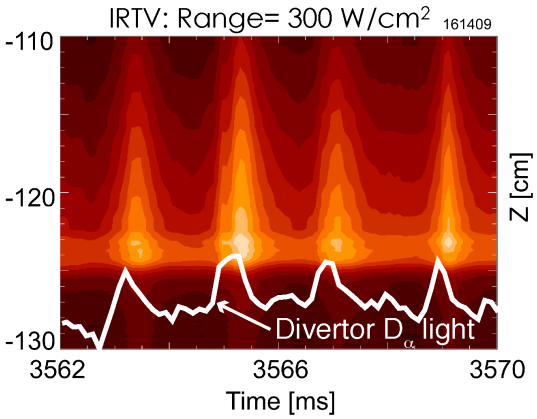

FIG. 7. Inner divertor heat flux (linear scale) measured by IR camera during "fuzzy ELMs".

exceeds unity at the top of the H-mode pedestal for both single fluid and two fluid calculations. Although it seems unlikely that strong magnetic stochasticity is generated in the hybrid case due to the presence of a significant temperature gradient, the calculation does suggest that a high density of magnetic islands can be generated at the top of the pedestal that can sustain ELM suppression over a wide contiguous range of q_{95}, as observed in experiment. In contrast, ITER Baseline plasmas typically have much smaller Chirakov parameter at the top of the pedestal with larger spacing of rationals.

Interestingly, the odd parity n=3 RMP used for ELM suppression in steady-state hybrids has only a minor impact on the pedestal pressure, as seen in Fig. 6(a), which likely explains the small ≈5% drop in H_{98y2} during ELM suppression. Figure 6(b) plots the peeling-ballooning stability boundary from the ELITE code [14] for two matched plasmas with and without ELM suppression. Both cases reside close to the low-collisionality peeling stability boundary (within errors), reflective of the minor impact of the RMP on the pedestal pressure. The plasma edge is not totally quiescent during the RMP phase but exhibits small amplitude bursts of particle and energy loss at ~500 Hz. These bursts or "fuzzy ELMs", seen on the photodiodes and IR camera (Fig. 7), are not well understood but do not pose a significant risk due to their high frequency and low peak heat flux, not exceeding 20% of the average heat flux.

The strength of the island "drive" can be explored by varying the NBI torque and assessing if ELM suppression can be maintained. In the ITER Baseline, a small reduction of beam torque leads to the loss of ELM suppression [15], indicative of the weak response of the highly-stable, negative-reluctance modes. However, a similar torque reduction in these hybrid plasmas reveals robust ELM suppression (although the ~500 Hz bursts of particle and energy loss remain) and a concomitant sameness in $\omega_{\perp e}$ at the top of the pedestal. This suggests that the beam torque is generally insufficient to compete with the JxB torque maintaining the islands at the top of the H-mode pedestal.

3. Fast Ion and Thermal Transport

Fast ion transport. High beta hybrids with central electron heating exhibit weaker energetic particle modes than similar plasmas without ECH. In discharges with NBI-only heating, a large number (8-10) of Alfvén eigenmodes (AE) are observed at high frequencies (100-250 kHz) in the cross-amplitude spectrum of density fluctuations from the CO_2 interferometer. The calculated Alfvén gap structure indicates these excited modes are in the TAE/EAE frequency range. This high frequency AE activity is suppressed when either ECCD or radial ECH is deposited near the plasma center, replaced by an intermittent fishbone-like mode that rapidly chirps down in frequency and has a dominant n=2 sideband that strongly couples to the m/n=3/2 mode.

For hybrid plasmas with NBI-only heating and strong AE activity, significant beam ion transport is needed in TRANSP modeling to match the experimental neutron rate. Figure 8(a) plots the ratio of the measured neutron rate to TRANSP neutron rate without anomalous beam ion diffusion for hybrids without (blue) and with (red) central ECCD. As shown in Fig. 8(b), TRANSP requires $D_{beam} \sim 1$ m^2/s to match the experimental neutron rate for the NBI-only ($P_{EC} = 0$) case. The anomalous beam ion transport increases in time correlated with increasing TAE/EAE activity. For a similar steady-state hybrid plasma with $P_{EC} = 2.3$ MW, the inferred D_{beam} is less than half of the NBI-only case.

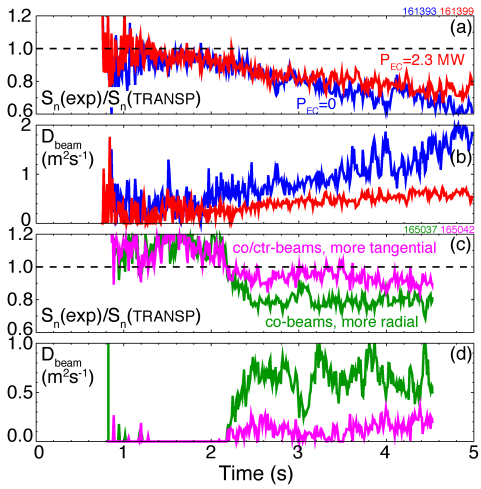

FIG. 8. (a) Neutron rate deficit and (b) beam ion diffusion coefficient for different ECH powers. (c) Neutron rate deficit and (d) beam ion diffusion coefficient for different mixes of beam sources.

While the fishbone mode with central ECCD causes less anomalous beam ion transport than AEs, it is not completely benign. Fortunately, the fishbone mode can be stabilized and the beam ion transport reduced to near zero by varying the mix of neutral beam sources. Figure 8(c) shows that the neutron rate from TRANSP without beam ion diffusion exceeds the measured neutron rate for a high beta hybrid using 10.7 MW of co-NBI (green) with nearly equal contributions from the "left" and "right" sources (the "right" sources inject more radially for co-injection). Changing the neutral beam mix by adding 2.4 MW of counter-NBI and reducing the "right" co-NBI power from 5.0 MW to 2.8 MW (magenta) eliminates the fishbone mode and brings the measured neutron rate into good agreement with the classical calculation (note that the ~10% variance between TRANSP and experiment early in the discharge may indicate a calibration issue). As seen in Fig. 8(d), TRANSP requires $D_{beam} \sim 0.7$ m^2/s in order to match the experimental neutron rate for the discharge with fishbones, but the inferred D_{beam} drops to near zero for the discharge without fishbones. While fishbones and AEs do not prohibit the $\beta_N = 3$ steady-state hybrid scenario in DIII-D, they give rise to a less optimistic projection to ITER.

Thermal transport. Transport analysis by TRANSP using a value of D_{beam} that best matches the experimental neutron rate shows that the electron thermal, ion thermal and momentum diffusivity profiles are identical with and without the odd parity n=3 RMP to within the error bars for steady-state hybrids at fixed NBI and EC power. The electron particle diffusivity is systematically 15% smaller for the RMP case, which is associated with the density profile being slightly more peaked than for the without RMP case.

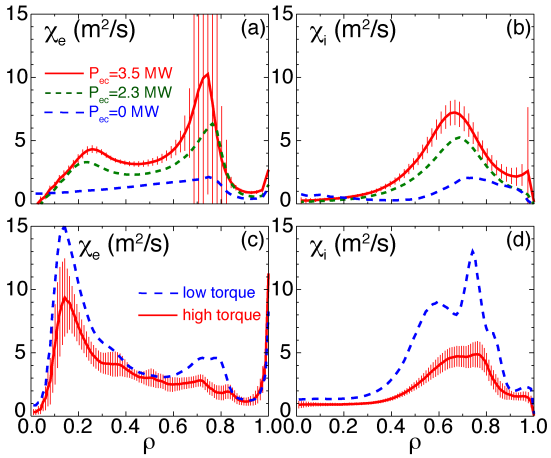

FIG. 9. (a) Electron and (b) ion thermal diffusivities for different ECH powers. (c) Electron and (d) ion thermal diffusivities for different NBI torques.

Transport analysis shows that the electron and ion thermal diffusivities jump higher in response to central electron heating. As seen in Fig. 9(a)-(b), both χ_e and χ_i increase across the plasma radius (except near the axis) with higher ECCD power. Since $\chi_e \approx \chi_i$, using equal amounts of electron and ion heating will naturally give $T_e \approx T_i$ in these plasmas. An important feature is that the confinement factor remains the same ($H_{98y2} = 1.4$) for the NBI-only ($P_{EC} = 0$) and $P_{EC} = 2.4$ MW hybrids despite the large increase in χ_e and χ_i for the latter case. This is because the higher thermal transport during ECCD is offset by the improved beam ion transport as the TAE/EAE modes are suppressed. If TRANSP is used to correct H_{98y2} for the effect of beam ion transport, then H_{98y2} decreases uniformly with increasing ECCD power, up to a 20% drop for $P_{EC} = 3.4$ MW, tracking the changes in χ_e and χ_i.

A scan of the NBI torque in high beta hybrids shows that thermal transport improves with higher plasma rotation (and thus higher E×B shear). Fully noninductive operation in DIII-D for $\beta_P \approx 2$ requires full use of the co-NBI sources, which also results in a large co-torque and rapid plasma rotation. To study the effect of plasma rotation on confinement in high beta hybrids, the beam torque is scanned from 8.6 N·m to 4.3 N·m at fixed NBI and ECH power (use of counter-NBI in the latter case means that these plasmas are no longer fully noninductive). As seen in Fig. 9(c)-(d), higher-torque hybrid plasmas have ≈25% lower χ_e and ≈50% lower χ_i compared to the lower-torque case. The H_{98y2} factor increases from 1.2 to 1.5 with higher beam torque. While Sec. 5 shows that ELM-suppressed, steady-state hybrids project to $Q_{fus} \geq 5$ in an ITER-sized plasma with $H_{98y2} = 1.2$, these experiments indicate that achieving even this modest H-factor may prove challenging in a low rotation plasmas.

4. Integration of High-β Hybrid and Radiating Divertor

A series of experiments in ELMy plasmas have integrated the high-beta hybrid scenario with an Argon-based radiating divertor and shown a factor of 2 reduction in the divertor heat flux while maintaining high performance. In addition to ELM suppression, future devices like ITER will need to incorporate a radiating divertor to reduce the peak heat flux in the divertor to an acceptable level and facilitate detachment of the divertor strike points. These "puff and pump" experiments rely on a strong ion flow into the divertor to impede the escape of the introduced impurities from the divertor into the main plasma. This flow is generated by a combination of upstream Deuterium gas injection and downstream particle exhaust. As seen in Fig. 10 for two ELMy hybrid plasmas with $\beta_N = 3.0$, the combination of

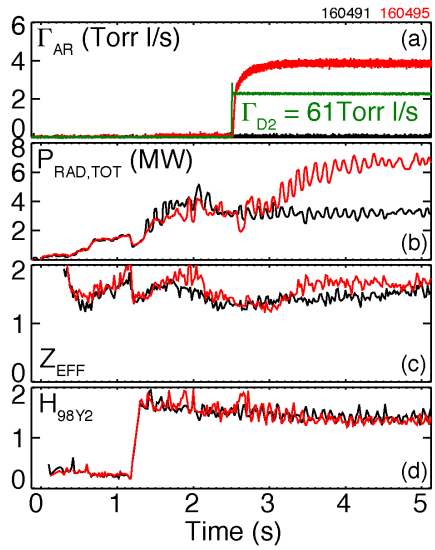

FIG. 10. Time history of hybrid with combined Ar and D_2 injection (red and green) and a similar hybrid without "puff and pump" (black).

Argon seeding and strong Deuterium puffing more than doubles the plasma radiative power, up to 55% of the input power, with only ≈10% increase in total Z_{eff}. In this experiment a double-null plasma shape is used to take advantage of the two outboard cryopumps connected to the top and bottom divertors. The ion $B\times\nabla B$ drift direction is towards the bottom of the machine and the plasma shape is slightly biased upwards (ΔR_{sep}=+7 mm). Deuterium gas puffing in the lower divertor sets up the strong ion flow and Argon is introduced into the upper divertor. These high heat flux experiments use ≈12 MW of combined ECH and NBI heating, with the radiative power increasing from 3.2 MW to 6.6 MW during the "puff and pump". High performance is maintained with Argon puffing as the thermal confinement factor of H_{98y2} = 1.35 is only 5% smaller than for a similar hybrid discharge without "puff and pump". A periscope offers a good view of the outer divertor strike points by an IR camera for measuring the divertor heat flux profile. As shown in Fig. 11, the peak heat flux in the upper, outer divertor falls by a factor of 2 (from 4.6 to 2.3 MW/m^2) for the Argon-based radiative divertor. At the same time a smaller decrease from 1.4 to 1.1 MW/m^2 is recorded in the lower, outer divertor, which handles less power since the plasma shape is biased upward.

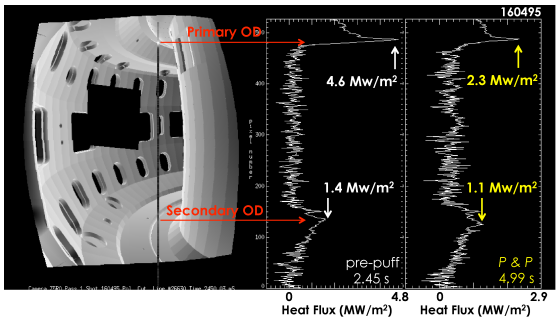

FIG. 11. Heat flux profile on divertor, measured by IR camera, for hybrids with and without a radiating divertor.

5. Extrapolation to ITER

The fully-noninductive hybrid scenario with ELM suppression discussed in this paper is a strong candidate for satisfying the ITER goal of demonstrating steady-state operation using noninductive current drive with Q_{fus} = 5, as described in reference scenario 4 (I_P = 9 MA, H_{98y2} = 1.3–1.5, P_{fus} = 500 MW) [16]. Figure 12 shows a RMP ELM-suppressed, steady-state hybrid discharge from DIII-D scaled to ITER's major radius and magnetic field strength while keeping fixed the dimensionless parameters β, ν* and q, as well as the plasma shape. This is essentially an extrapolation to smaller ρ* except that ITER will have a different mix of ion species and a higher thermal energy fraction (which reduces ν* by a factor of 2 and raises the bootstrap current fraction compared to DIII-D). In Fig. 12, the plasma current scaled to ITER is 9.6 MA, the scaled density is ≈25% above the Greenwald density, and the average fusion power is 460 MW during the high beta phase ($\langle\beta\rangle$ = 2.5%). The time base in Fig. 12 is determined by multiplying the time in DIII-D by the ratio of the current relaxation times (τ_R = 1.9 s in DIII-D, 245 s in ITER).

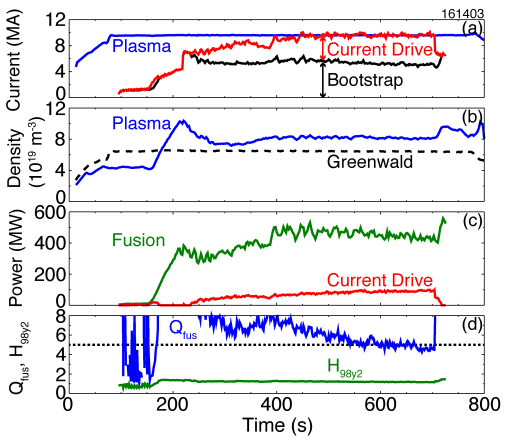

FIG. 12. ELM-suppressed, steady-state hybrid discharge from DIII-D scaled to ITER's major radius and magnetic field strength with dimensionless parameters held fixed (except ρ).*

The external power needed to obtain full current drive in Fig. 12 is determined using the current drive efficiencies from the ITER Physics Basis [17]. Expressed as a dimensionless efficiency $\zeta = e^3 I_{CD} n_e R/\varepsilon_o^2 P_{CD} T_e$, the theoretical current drive efficiency for central EC and FW is ζ_{EC} = 0.41, while for high-injection-energy neutral beams ζ_{NB} = 0.52. Figure 12 shows that ≈4.2 MA needs to be driven from external sources during the steady-state phase; for a 50-

50 mix of neutral beam and RF sources, this requires a current drive power of ≈85 MW. Assuming that no additional external power is needed to obtain $\langle\beta\rangle = 2.5\%$, this gives $Q_{fus} \approx 5.4$ and $H_{98y2} \approx 1.2$ averaged over the high beta phase. An alternative calculation of the confinement needed to satisfy power balance in Fig. 12 can be made by recalling that this constitutes a ρ* scan from DIII-D to ITER. Ignoring the change in ion mass and collisionality, and implicitly assuming the Mach. no. remains the same, a transport scaling of $\chi = \chi_B \rho_*^{0.47}$, i.e., between Bohm and gyro-Bohm, is needed to achieve $Q_{fus} = 5.4$ in ITER based upon the DIII-D transport levels.

6 Conclusions

These experiments in DIII-D demonstrate that the hybrid scenario with central current drive, RMP ELM suppression and radiative divertor is an attractive regime for achieving the fusion performance goals in steady-state scenarios in ITER. For the first time, a high-beta, fully-noninductive hybrid in the ITER similar shape is successfully integrated with ELM suppression by applying an odd parity n=3 RMP with little confinement degradation. While central electron heating is found to increase thermal transport, it also can substantially reduce the deleterious effect of energetic particle modes compared to NBI-only cases in DIII-D. Experiments in high beta hybrids find that an Argon-based radiating divertor can reduce the divertor heat flux by a factor of 2 while maintaining high performance. The characteristics of these ELM-suppressed plasmas are consistent with strong edge kink amplification of positive reluctance modes combined with the high density of rational surfaces at the top of the pedestal. These properties are quite unlike those of low beta plasmas and the results suggest that ELM suppression by RMPs may be more effective in steady-state reactors than in present day inductive experiments.

This material is based upon work supported by the U.S. Department of Energy, Office of Science, Office of Fusion Energy Sciences, using the DIII-D National Fusion Facility, a DOE Office of Science user facility, under Awards DE-FC02-04ER54698[1], DE-AC02-09CH11466[2], DE-FG02-04ER54761[3], DE-AC52-07NA27344[4], DE-FG02-07ER54917[5], and DE-FG03-97ER54271[7]. DIII-D data shown in this paper can be obtained in digital format at https://fusion.gat.com/global/D3D_DMP.

References

[1] F. TURCO et al., Phys. Plasmas **22**, 056113 (2015)
[2] C.C. PETTY et al., Nucl. Fusion **56**, 016016 (2016)
[3] T.C. LUCE et al., Nucl. Fusion **54**, 013015 (2014)
[4] M.R. WADE et al., Nucl. Fusion **45**, 407 (2005)
[5] J.E. KINSEY et al., Nucl. Fusion **45**, 450 (2005)
[6] A. LOARTE et al., Nucl. Fusion **54**, 033007 (2014)
[7] T.C. LUCE et al., Nucl. Fusion **54**, 093005 (2014)
[8] P. PIOVESAN et al., EX/1-1, this conference
[9] C. PAZ-SOLDAN et al., Phys. Rev. Lett. **114**, 105001 (2015)
[10] N.C. LOGAN et al., Phys. Plasmas **23**, 056110 (2016)
[11] R. NAZIKIAN et al., Phys. Rev. Lett. **114**, 105002 (2015)
[12] J.-K. PARK et al., Phys. Plasmas **14**, 052110 (2007)
[13] N.M. FERRARO and S.C. JARDIN, J. Comput. Phys. **228**, 7742 (2009)
[14] P.B. SNYDER et al., Phys. Plasmas **9**, 2037 (2002)
[15] C. PAZ-SOLDAN et al., EX/1-2, this conference
[16] C. GORMEZANO et al., Nucl. Fusion **47**, S285 (2007)
[17] ITER Physics Basis, Nucl. Fusion **39**, 2137 (1999)